Mapping quantum dot-in-well structures on the nanoscale using the plasmon peak in electron energy loss spectra

A. M. Sánchez,[1] R. Beanland,[2,*] M. H. Gass,[1] A. J. Papworth,[1] P. J. Goodhew,[1] and M. Hopkinson[3]
[1]*Department of Engineering, University of Liverpool, Liverpool L69 3GH, United Kingdom*
[2]*Bookham Technology, Caswell, Towcester, Northants, NN12 8EQ, United Kingdom*
[3]*Department of Electronic and Electrical Engineering, University of Sheffield, Sheffield S1 3JD, United Kingdom*
(Received 24 December 2004; revised manuscript received 27 May 2005; published 16 August 2005)

Plasmon energy losses experienced by fast electrons passing through a thin specimen are readily measured using electron energy loss spectroscopy. We describe a simple model of the shape and energy of the single scattering distribution plasmon peak, which relates the energy loss spectrum to the material parameters of average band gap $\bar{E}_g$, lattice parameter a, core ion dielectric constant ε_c, and plasmon lifetime τ. This model is used to interpret maps of plasmon energy and full width at half maximum taken from an InAs/$In_xGa_{1-x}As$ quantum dot-in-well structure. We find that the bulk plasmon peak shifts are mainly determined by the strain in the structure, which may provide a new means of mapping strain on the nanoscale. The regions of maximum plasmon peak width appear to correspond to regions of high strain gradient. It is possible to separate the effects of plasmon lifetime from the other factors, leaving a parameter which is a combination of $\bar{E}_g$, a, and ε_c. We have been able to map this parameter with a spatial resolution of a few nm.

DOI: 10.1103/PhysRevB.72.075339 PACS number(s): 78.67.Hc, 82.80.Pv, 71.45.Gm, 68.37.Lp

I. INTRODUCTION

Structures based on InAs quantum dots embedded in $In_xGa_{1-x}As$ quantum wells (so-called DWELL structures[1]) offer the potential for high-performance lasers at the 1.3 μm waveband which have potential for low cost sources for metropolitan access networks. The InAs DWELL is a highly complex heterostructure and a knowledge of its electronic structure under the influence of variable structural parameters is of great interest for the further development of its optoelectronic properties. In the DWELL structure, the quantum dot size, shape, and the compositional profile of both the dot and the quantum well are the key structural parameters and knowledge of these would allow, in principle, the electronic structure to be derived. However, even if the structure is accurately known, the resulting calculations are highly complex and there would be great benefit in measuring the electronic properties by direct means.

Transmission electron microscopy (TEM) provides a visualization of the sample structure, since it is possible to reveal the position of atomic columns using the high-resolution mode.[2,3] High-resolution electron microscopy (HREM) is well established for atomic-scale imaging of a wide variety of materials. Quantitative information at the atomic scale, such as the local strain, can be also obtained.[4] High-resolution electron energy loss spectroscopy (HREELS), energy dispersive x-ray analysis (EDX), or high-angle annular dark-field (HAADF) techniques can be used to obtain the composition of each column of atoms, although often this is not straightforward as it depends on the atomic properties which are measured. HREELS provides data pertaining to the vibrational energy of molecules,[5] while HAADF imaging is related to the atomic number contrast by detecting large-angle scattering of the incident electrons.[6] On the other hand, electron energy-loss spectroscopy (EELS) can provide an insight into dielectric properties of the material and has been used to investigate electronic structure in III-V heterostructures.[7–10]

Here, we describe the measurement of low-loss electron energy loss spectra from a quantum dot heterostructure and describe the dielectric properties of the semiconductor material following the Drude-Lorentz model. This relationship is then used to interpret low-loss EELS maps of nanometer scale semiconductor heterostructures.

The range between 0 and 100 eV in the electron energy loss spectrum contains information about the interactions between the incident electron beam and the solid.[11] This low-loss region of the EELS spectrum contains an elastic, or zero-loss, peak followed by single or multiple scattering events specific to the material. After the zero-loss peak, the major feature in this region of the spectrum corresponds to the bulk plasmon. The bulk plasmon is a collective oscillation of the loosely bound electrons, which runs as a longitudinal wave through the volume of the crystal with a characteristic frequency ω_p. The excitation of this collective oscillation, or plasma, in the solid is necessarily quantized, so we can consider the plasmon as equivalent to a pseudoparticle of energy[12] $E_p = \omega_p$. Here, we are primarily interested in the information which can be obtained by examining the plasmon energy and width and how these vary in nanometer-scale semiconductor heterostructures. We thus give a brief description of the material-related parameters which are responsible for the plasmon peak properties.

The simplest approach is to ignore the complicating factors of band structure and the bonds between atoms and consider the valence electrons to be a free-electron gas. A simple derivation[13] shows that the plasma frequency in this case is,

$$\omega_p = \left(\frac{ne^2}{\varepsilon_0 m_0} \right)^{1/2}, \tag{1}$$

where n denotes the density of electrons, e is the electron charge, ε_0 is the permittivity of free space, and m_0 is the

mass of the electron. This equation usually gives a plasma frequency within a few percent of observed values for materials whose valence bands are well removed from any core states. The energy of a plasmon excited in a free electron gas is thus

$$E_p = \omega_p = \left(\frac{ne^2}{\varepsilon_0 m_0} \right)^{1/2}. \tag{2}$$

Note that the plasmon energy is expected to be proportional to $a^{-3/2}$, where a is the lattice parameter of a cubic material, through the electron density n.

Equation (2) is based on the assumption that there is no damping present in the free electron gas, in which case the energy loss spectrum will be a delta function at E_p. A more realistic situation is that the resonance excited in the free electron gas is damped. As is usual in a damped resonant system, the resonance now extends over a range of frequencies, with a wider range corresponding to stronger damping. The plasmon peak in an energy loss spectrum will thus broaden and shift from the undamped value ω_p as damping increases. In quantum particle terms, the plasmon is allowed to decay, the lifetime of the particle τ being inversely proportional to the amount of damping. The decay pathway is determined by the interband transitions which have a nonzero transition probability at the plasmon energy, which will vary both with material composition and the details of a heterostructure.

The energy loss of a fast electron passing through a damped free electron gas is usually framed in terms of the dielectric function, which relates the electric field of the electron (parallel to the electron trajectory) to the induced field in the gas through its polarizability. To account for the different phases of the electric field (**E**), polarization (**P**), and displacement (**D**) in Gauss's law for dielectrics, $\mathbf{D}=\varepsilon_0\mathbf{E}+\mathbf{P}=\varepsilon\varepsilon_0\mathbf{E}$, a complex notation is introduced, with the dielectric function having the form $\varepsilon(\omega)=\varepsilon_1(\omega)+i\varepsilon_2(\omega)$. This approach is familiar to most through the interaction of a photon with a solid, the difference being that the electric field of a photon is transverse to its direction of propagation, whereas that of an electron is longitudinal. This difference completely changes the part of the dielectric function that affects the energy loss spectrum for electrons in comparison with the absorption of photons. Applying a condition of continuity at the interface where the electron enters the solid shows that the induced electric field in the material is reduced by a factor of $1/\varepsilon$ in comparison with that outside the material in vacuum. This results in an energy loss function of the form[11,12,14]

$$I(\omega) \propto \mathrm{Im}\left(\frac{-1}{\varepsilon(\omega)} \right) = \mathrm{Im}\left(\frac{\varepsilon_2(\omega)}{\varepsilon_1^2(\omega)+\varepsilon_2^2(\omega)} \right), \tag{3}$$

whereas for photons the absorption is proportional to $\mathrm{Im}[\varepsilon(\omega)]$. Now, in the case of a damped free electron gas, the dielectric function has the form[11]

$$\varepsilon(E) = 1 - \frac{E_p^2}{E^2 + iE\Gamma}, \tag{4}$$

where $\Gamma = 1/\tau$, τ being the characteristic relaxation time for the plasmon. Using this in (3) gives

$$I(E) \propto \frac{E\Gamma E_p^2}{(E_p^2 - E^2)^2 + E^2\Gamma^2}, \tag{5}$$

with a maximum at an energy E_{max}, given by

$$E_{\max} = \left(\frac{2E_p^2 - \Gamma^2 + \sqrt{(2E_p^2 - \Gamma^2)^2 + 12E_p^4}}{6} \right)^{1/2}, \tag{6}$$

i.e., damping shifts the plasmon peak to slightly lower energies.

Two further modifications are necessary to have a realistic description of a plasmon in a semiconductor material. First, the dielectric function ε_c of the core electrons and positive ions, which do not participate in the resonance, must be taken into consideration. Since they do not affect the phase of the plasmon, ε_c can be taken as having no imaginary component at the plasma frequency, and so we replace the value of unity on the right-hand side of Eq. (4) with ε_c, giving

$$\varepsilon(E) = \varepsilon_c - \frac{E_p^2}{E^2 + iE\Gamma}. \tag{7}$$

The second modification was proposed by Horie,[15] who suggested that an electron plasma in a semiconductor material will have the frequency

$$(\omega_p')^2 = (\omega_p)^2 + \bar{E}_g^2, \tag{8}$$

where ω_p' is the modified electron plasma frequency, $\bar{E}_g$ denotes an "average" band gap, i.e., corresponding to the maximum absorption of an electromagnetic wave, and ω_p is the free electron plasma frequency. Combining this concept with Eq. (7) gives the following form for the dielectric function, as previously given by Frölich[16]:

$$\varepsilon(E) = \varepsilon_c + \frac{E_p^2}{(\bar{E}_g^2 - E^2) - iE\Gamma}. \tag{9}$$

Giving the energy loss function,[17]

$$I(E) \propto \frac{E\Gamma E_p^2}{\varepsilon_c^2\left[\left(\bar{E}_g^2 + \frac{E_p^2}{\varepsilon_c} - E^2 \right)^2 + E^2\Gamma^2 \right]} \propto \frac{E}{(E_p'^2 - E^2)^2 + E^2\Gamma^2}, \tag{10}$$

where E_p' is the modified electron plasma energy, given by

$$E_p'^2 = \bar{E}_g^2 + E_p^2/\varepsilon_c. \tag{11}$$

It has been shown[12,17] that a factor of $\ln(2E_0/E)$ should also be introduced in Eq. (10) to account for the integration of momentum transfer from the primary electron to the plasmon over the solid angle of collection, determined by the collection aperture. However, this term is slowly varying in the region of interest here, and has little effect on the energy or

FWHM of the plasmon peak. Therefore, for clarity, it is neglected here.

Since (10) has the same form as (5), with E_p replaced by E'_p, in the SSD, the plasmon energy in a semiconductor material is

$$E_{\max} = \left(\frac{2E_p'^2 - \Gamma^2 + \sqrt{(2E_p'^2 - \Gamma^2)^2 + 12E_p'^4}}{6} \right)^{1/2}. \quad (12)$$

The maximum in the SSD is thus dependent on E'_p and the damping constant Γ. The energy loss function full width at half-maximum (FWHM), ΔE, depends only on the damping constant, and is simply

$$\Delta E = \Gamma. \quad (13)$$

Rearranging Eq. (12) to solve for $E_p'^2$ gives

$$E_p'^2 = \bar{E}_g^2 + E_p^2/\varepsilon_c = E_{\max}\sqrt{4E_{\max}^2 + \Gamma^2} - E_{\max}^2. \quad (14)$$

Equations (11), (13), and (14) describe a relationship between the material properties of band gap, lattice parameter, core dielectric constant, plasmon lifetime, and experimentally accessible parameters of the plasmon peak width and energy. Although the dielectric parameters can be obtained from optical experiments for bulk materials, EELS can be used on a nanoscale, allowing unprecedented access to the dielectric properties of semiconductor heterostructures. These equations provide a framework which may allow spatial mapping of E_{max} and FWHM to be interpreted as maps of the component parts of the dielectric function. Some caution must be exercised, however, since there are effects which can cause changes in E_{max} and FWHM in single crystal semiconductor materials without changes in composition.[17] In particular, the plasmon peak is known to broaden and shift to higher energies in very thin specimens (less than approximately 25 nm). There are several mechanisms which may be responsible for this effect. Surface plasmons, with energy approximately half that of the bulk plasmon, are generated at the sample surfaces. This decay pathway may be more significant in very thin specimens and hence may increase the FWHM of the bulk plasmon peak. Quantum confinement effects in a very thin specimen will also increase the probability of interband transitions that can provide plasmon decay pathways; the band gap also increases as material dimension decreases[18], giving a mechanism for the increase in E_{max}. Finally, the wavelength of a plasmon is on the order of a few nm, and so confinement of the plasmon itself may also occur. Although we have avoided the very thin region of the specimen and so these effects do not apply to the bulk materials in the specimen, they may be relevant where the heterostructures themselves are of nanoscale. The bulk plasmon energy also depends on the electron wave vector, $\mathbf{q}$, since this determines the momentum transferred to the plasma. This can be neglected when $|\mathbf{q}|=0$, but significant changes in the energy loss spectrum are observed due to dispersion,[19,20] particularly when $|\mathbf{q}|>9$ nm^{-1}. In our case, since we use a small aperture centered on the undiffracted beam, we would expect the majority of energy loss transitions to be around $|\mathbf{q}|=0$. However, if a diffraction event occurs prior to excitation of a plasmon, it is possible for significant momentum transfer to occur.[11]

II. EXPERIMENTAL

The sample chosen for investigation was a self-assembled InAs/GaAs quantum dot heterostructure. Deposition was performed in a VG Semicon V80H molecular beam epitaxy system on Si-doped GaAs (100) substrates. Three layers of InAs dot-in-well (DWELL) structures were grown at 510 °C with 50 nm GaAs spacer layers between. Each DWELL layer consisted of 2.9 monolayer InAs quantum dots grown on 2 nm $In_{0.15}Ga_{0.85}As$, capped by 1 nm $In_{0.2}Al_{0.8}As$, further followed by 5 nm $In_{0.15}Ga_{0.85}As$. The 1 nm $In_{0.2}Al_{0.8}As$ layer was used to improve the optical confinement of the quantum dot heterostructure. The three-layer DWELL structure was embedded between 200 nm GaAs layers, which were further confined by $Al_{0.4}Ga_{0.6}As$ layers.

Cross-section TEM specimens were prepared in the usual manner,[21] i.e., by mechanical grinding to below 20 μm and mechanical polishing using 1 μm diamond suspension on a soft nap pad. The specimens were ion-milled to electron transparency using Ar^+ ions at 6 kV and a beam incidence angle of 3° (uncooled). A final low-energy "clean" of the sample at 2 kV was employed to minimize amorphous surface layers. Conventional TEM was carried out on a JEOL 100CX microscope operating at 120 kV close to the $[110]_{GaAs}$ zone axis. Further investigations were carried out using a VG HB601 UX FEG-STEM operating at 100 kV. The STEM was equipped with the Gatan ENFINA™ parallel electron energy loss spectrometer (PEELS) system. The EELS data was acquired using a collection aperture with semi-angle $\beta=1.34$ mrad. This is a relatively small collection aperture in comparison with previous work,[22–24] and was used since it gives a significantly increased energy resolution, determined to be 0.35 eV as measured from the FWHM of the zero-loss peak. A typical EELS map contained 600 low-loss spectra. The acquisition time for each spectrum was 300 ms giving a total acquisition time of approximately 10 min. Comparison between diffraction patterns taken before and after analysis showed no discernible change in the material that could be caused by beam damage.

III. RESULTS

Figure 1 shows a typical dark field 002 image. The 002 reflection is compositionally sensitive, with the contrast being roughly proportional to the square of the difference in average group III and V atomic number.[25,26] The InAs quantum dots appear as bright regions, 10–15 nm wide and 5–8 nm high, in a dark layer of $In_xGa_{1-x}As$, with gray GaAs barriers between each DWELL structure. The capping layer of $In_yAl_{1-y}As$ appears as a thin bright line in the lower part of the dark $In_xGa_{1-x}As$ well, but is generally indistinguishable from the InAs where it lies on top of the dots.

The InAs DWELL structure is also shown in the annular dark field STEM image of Fig. 2. A spectrum image (SI) of the low-loss spectrum was recorded in the boxed area in Fig. 2, containing one of the quantum dots. The effects of spatial

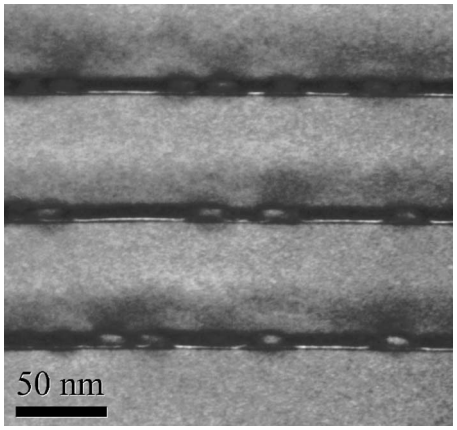

FIG. 1. Dark field 002 TEM image, showing the InAs DWELL layers.

drift have been corrected during the acquisition of the SI. The growth direction is vertical in both in Figs. 1 and 2.

Single scattered distribution (SSD) spectra were obtained by removing the zero-loss peak and plural scattering from the low-loss region of the EELS spectra using a Fourier logarithmic deconvolution. A typical plasmon peak from GaAs after this procedure is shown in Fig. 3; both the energy (15.98 eV) and FWHM (4.19 eV) are in good agreement with published values.[17] A least-squares fit of Eq. (10) to the experimental data is shown as a dotted line. It can be seen that an excellent fit is obtained over the central part of the peak. The features on the right of the peak are due to the Ga 3*d* core transitions and were not included in the fit. The energy of the undamped free electron plasma [Eq. (1)] is also shown as a dash-dot line. The mean energy gap $\bar{E}_g$ was taken to be the energy corresponding to the maximum absorption of photons, i.e., 5.0 eV,[27] and the damping constant and core dielectric constant were taken as free parameters in the fit. This gave $\Gamma=4.19$ eV ($\tau=1.57.10^{-16}$ s) and $\varepsilon_c=1.041$.

By fitting a Gaussian function to the plasmon peak it is possible to determine energy with a resolution better than the

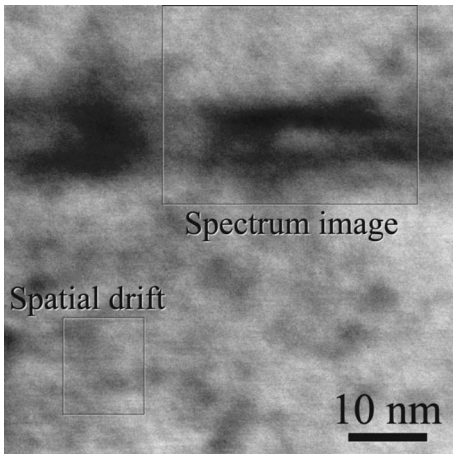

FIG. 2. STEM dark field image of one layer in the InAs/GaAs heterostructure. The area analyzed by EELS is marked as "spectrum image." Spatial drift corrections were measured, and corrected during acquisition of the EELS data.

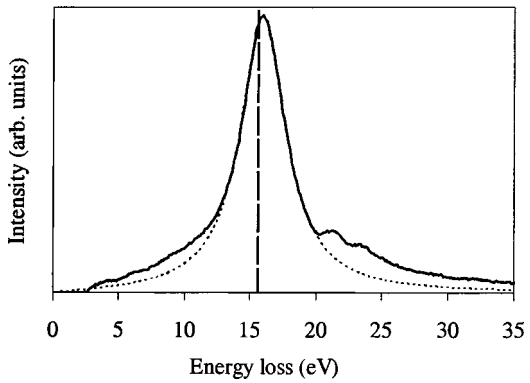

FIG. 3. A measured SSD plasmon peak in bulk GaAs (bold) and a least squares fit (dotted) according to Eq. (12).

0.1 eV between data points in Fig. 3.[28] The variation in plasmon energy has been calculated using a map of a relatively large area of GaAs from which 800 EELS spectra were recorded. In this data set the standard deviation of the fitted plasmon energy was 7 meV.

Figure 4(a) shows a map of the plasmon energy E_{max} in the region indicated on Fig. 2, with higher E_{max} represented by brighter pixels. The InAs quantum dot is clearly visible as a darker region; E_{max} in SSD spectra thus shifts to a lower energy in the area corresponding to the InAs quantum dot and in the quantum well region. Also marked are lines *A*, *B*, and *C*, which mark the data used for the line plots of Figs.

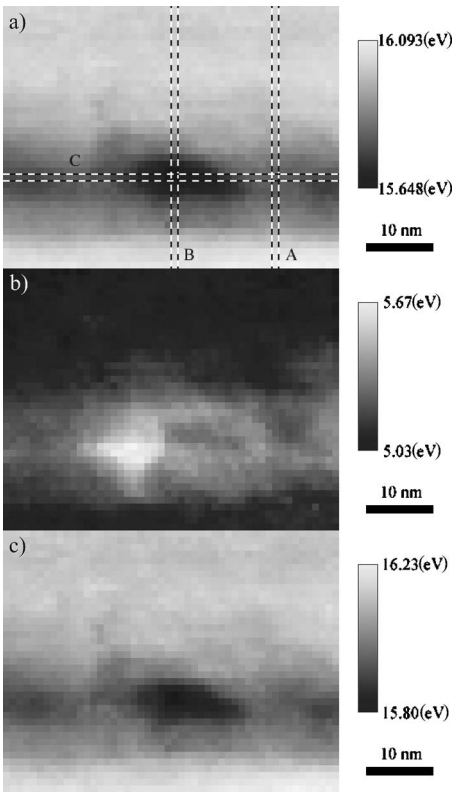

FIG. 4. (a) A map of plasmon energy $E_{\max}$ for the region shown in Fig. 2. Also marked are lines which show the position of the data *A*, *B*, and *C* plotted in Fig. 5. (b) A map of FWHM Γ and (c) E_p', extracted from the data in (a) and (b).

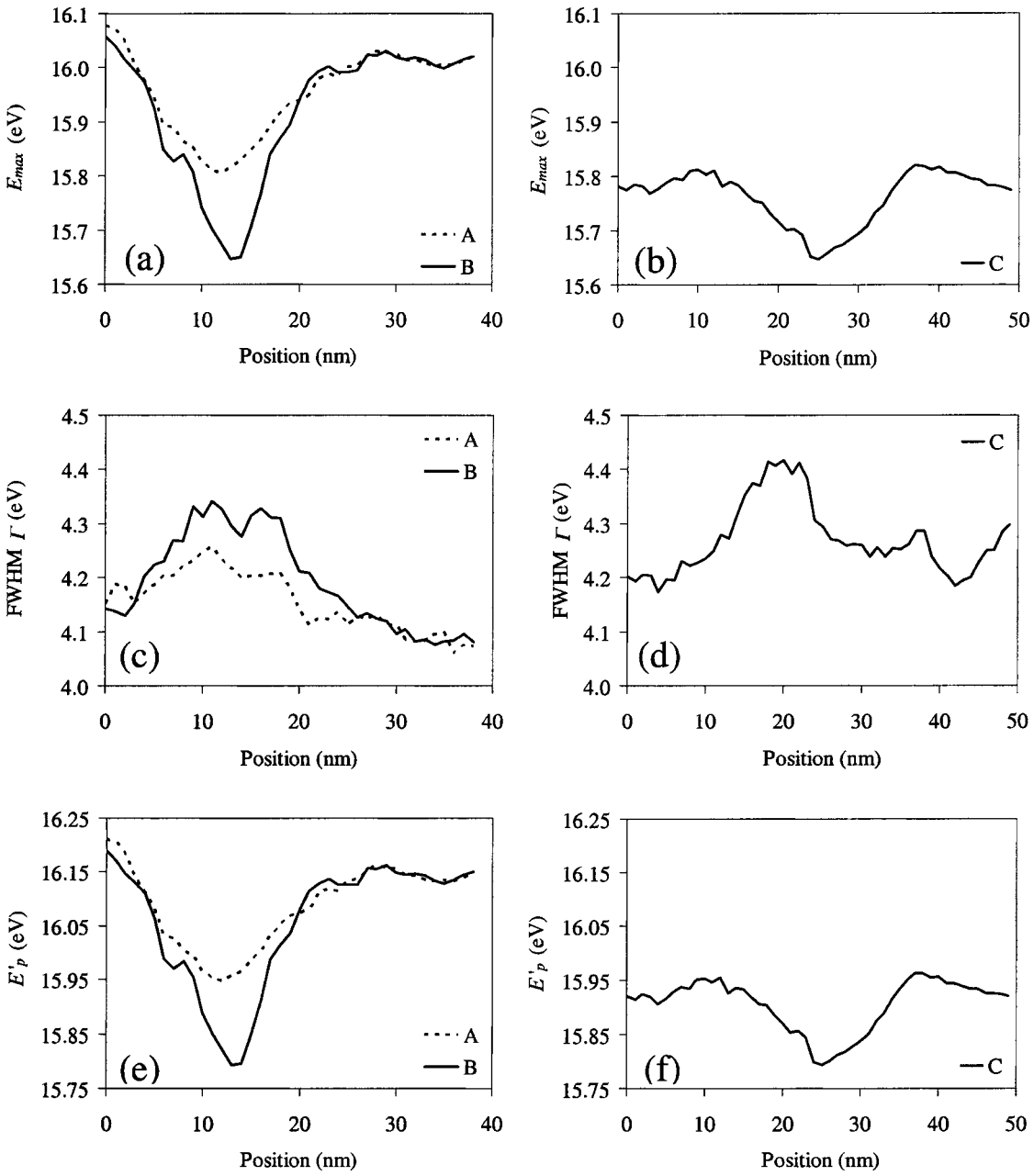

FIG. 5. Data extracted from Fig. 4 along the lines *A*, *B*, and *C* shown in Fig. 5(a). (a), (b) energy $E_{\max}$; (c), (d) FWHM Γ; and (e), (f) the parameter E_p'.

5(a) and 5(b). A map of FWHM Γ is shown in Fig. 4(b), with brighter pixels corresponding to larger Γ; line plots are shown in Figs. 5(c) and 5(d). Finally, a map of E_p', derived by applying Eq. (14) to Figs. 4(a) and 4(b), is shown in Fig. 4(c), with line plots in Figs. 5(e) and 5(f).

These images and graphs show how plasmon peak mapping can be applied on a nanoscale, with significant changes in both E_{max} and Γ as the composition of the material varies. The energy, E_{max}, decreases by $\sim$0.2 eV in the $In_xGa_{1-x}As$ well, and up to $\sim$0.4 eV in the InAs dot. Interestingly, the maximum Γ does not occur at the same position as the maximum shift in energy, lying to one side of the dot. Finally, E_p' follows a similar trend to E_{max}, but is shifted upwards in energy by approximately 0.15 eV.

IV. DISCUSSION

The maps of E_{max}, Γ, and E_p' show details that are related to the different materials present in the heterostructure. Although it is not possible to say which of the three underlying parameters E_p, $\bar{E}_g$, and ε_c are changing, we can use the model to predict the changes in E_p' we might expect for the different materials and compare the predicted values with the experimentally observed ones. The simplest way to do this is to vary each parameter independently, as shown in Fig. 6.

From Eq. (2) it is clear that the only material-dependent parameter in E_p is the electron density—which depends on the lattice parameter—and so we show the change in E_p' as a function of change in lattice parameter in Fig. 6(a), with

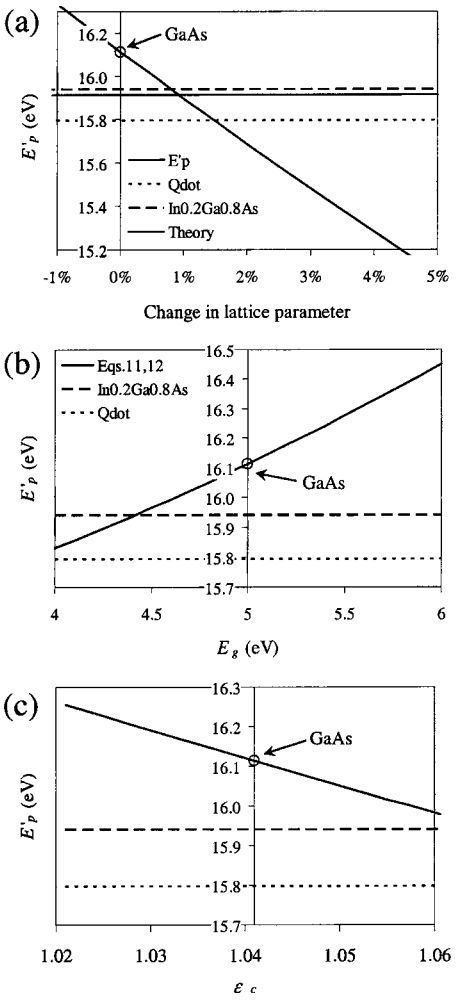

FIG. 6. Variation in plasmon peak position predicted from Eqs. (11) and (12) as a function of change in (a) lattice parameter, (b) E_g, (c) ε_c, and (d) Γ. In all cases the theoretical change is shown as a thick solid line: the measured peak position of GaAs is shown as a horizontal dashed line which crosses the theoretical curve in the center of the data range. The plasmon energy in the quantum dot is shown as a dashed line, and that in the $In_{0.2}Ga_{0.8}As$ well is shown as a line of diamond data points. The expected plasmon energy in the well is shown in (a) as a line of square data points.

positive values corresponding to increased lattice parameter. The solid line shows the predicted variation in E'_p as a function of change in lattice parameter, holding $\bar{E}_g$ and ε_c constant. The measured value for GaAs is shown by a circle; the measured value in E'_p in the $In_{0.2}Ga_{0.8}As$ well, 15.94 eV, is shown by a dashed line, and that in the quantum dot, 15.80 eV, is shown as a dotted line. The first point to note is that strain has a large effect on E'_p; an increase in lattice parameter of 1% shifts E'_p downwards by about 0.2 eV. The predicted value of E'_p for coherently strained $In_{0.2}Ga_{0.8}As$, 15.91 eV, is shown as a gray line, which is in fair agreement with the measured value. However, we would expect much larger changes in E'_p for the quantum dot, since the strain in a coherent InAs dot should be around 7% with respect to GaAs whereas the measured E'_p only requires a strain of 1.5%. The difference in band gap will have some influence, although this should in fact increase the shift in E'_p still further as shown below. Therefore the change in E'_p for the quantum dot is far smaller than expected. This must be at least in part due to the projection effect; the quantum dot only takes up about 15 nm of the approximately 40 nm thick specimen, and since the peak width is much larger than the observed shift, a large shift in E'_p in the dot may be masked by the material making up the rest of the specimen thickness. However, there may also be some other effect which causes a peak shift in the opposite sense. For example, the dot could be considered to be a separate entity with dimensions of the order of 15 nm; a shift to higher energies is also seen in TEM specimens with similar dimensions. It could also be argued that the lower than expected shift in E'_p is due to an inability to generate a plasmon sufficiently small to exist solely within the quantum dot.

Figure 6(b) shows the change in E'_p as a function of change in average band gap $\bar{E}_g$. For this materials system the influence of changes in band gap is much smaller than that due to changes in lattice parameter; the optically measured value for unstrained bulk InAs of 4.6 eV should give a change of −1.1 eV. However, the InAs is coherently strained and its band gap would be expected to be larger than that of bulk material, giving an even smaller change in E'_p. In any case, a shift in E'_p due to changes in band gap should add to that due to changes in lattice parameter and does not explain the relatively low value of E'_p we observe. Figure 6(c) shows the peak shift due to changes in core dielectric constant ε_c. At present the precise range of this parameter is not clear, however we note that the influence on E'_p appears to be relatively small.

All of the graphs shown in Fig. 6 indicate that despite the complexity of Eqs. (11) and (12), the predicted change in E'_p essentially varies in a linear manner as a function of lattice parameter, band gap, and core dielectric constant. Using a linear fit to the calculated curves gives the following phenomenological relationship for this materials system:

$$E'_p = 16.11 - 21.90\phi + 0.31(\bar{E}_g - 5.0) - 7.0(\varepsilon_c - 1.041), \tag{15}$$

where ϕ is the change in lattice parameter.[17]

This simple approach shows that although it may be possible in principle to extract dielectric properties from a more sophisticated analysis of the loss function, i.e., by performing a Kramers-Kronig analysis and obtaining the full dielectric function, the dominating factor determining peak shift in strained semiconductor systems is the change in electron density via the lattice parameter; changes due to band structure are a second-order effect. This opens up the possibility of using plasmon peak position maps as a measure of strain on a nanoscale, although in this case care must be taken to account for the band structure to obtain accurate results, and further work is needed to determine whether the lower than expected shift seen in the quantum dots can be explained solely by the projection effect. Here, we have only been able to remove the effect of damping to produce the map of E'_p; we anticipate that it will be possible to extract the different

parameters more readily once a Kramers-Kronig analysis has been performed.

The map of the plasmon peak FWHM Γ also shows some interesting and to some extent unexpected features. The maximum of Γ, and hence of the minimum plasmon lifetime, appears to lie as a halo around the dot rather than at the dot itself in Fig. 4(b). This does not correspond to the material with the smallest band gap, the highest strain, or the largest changes in composition through the specimen. It does, however, correspond to the maximum strain gradient in the material resolved perpendicular to the beam direction. This may be caused by two factors. First, a strain gradient will result in several plasmon energies as shown in Fig. 6(c), giving a broader peak. Second, if the distortion in the crystal is sufficient to tilt it locally into a strong diffraction condition, a significant fraction of electrons may experience an elastic diffraction event prior to a plasmon energy loss event. In this case the diffracted electrons will have a significant component of momentum perpendicular to the optic axis and the assumption that $|\mathbf{q}| \approx 0$ will no longer be valid. Since plasmon peak energy and FWHM both increase[11] as a function of $\mathbf{q}$, we may expect an increase in Γ in regions exhibiting strong diffraction contrast.

The resolution of the maps of plasmon peak parameters is matter of some interest. Although the electron probe has an estimated diameter of only 0.8 nm (full width 1/10 maximum), the resolution of the plasmon peak parameter maps will be determined by the size of the plasmon, which may be larger than the electron probe. Energy losses have also been measured in an electron beam which passes through vacuum, but close to a specimen, due to the finite electric field which lies outside the material,[29] and similar effects may also occur in heterogeneous specimens. While this specimen is not ideal for a measurement of resolution, it is interesting to compare the map of E_p', Fig. 4(c), with the dark field 002 image of Fig. 1 and the annular dark field image of Fig. 2. The dark field 002 image has a resolution better than 2 nm, as is evident from the clearly defined 2 nm thick $In_{0.15}Ga_{0.85}As$ (dark) and 1 nm thick $In_{0.2}Al_{0.8}As$ (bright) layers at the bottom of each quantum well. Figure 7 shows a comparison between the different types of image, with a scaled line plot of dark field 002 intensity I_{002} below, and a similar line from the ADF image above, the line of E_p'. It is clear from this plot that the resolution of the E_p' map is at least as good as the ADF image and is comparable to, or slightly lower than, that of the dark field 002 image. Further work is needed to determine the influence of the lateral extent of the plasmon on the measured parameters. Despite these limitations, it is very obvious that the properties measured by plasmon peak parameter maps—the combined effect of lattice parameter, $\bar{E}_g$, and ε_c—have a resolution which is orders of magnitude better than any other technique.

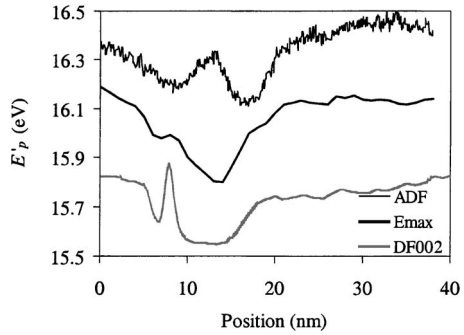

FIG. 7. Comparison of the spatial resolution of the map of the parameter E_p', the dark field 002 image of Fig. 1, and the ADF image of Fig. 2. The resolution of all images is of the order of a few nm.

V. SUMMARY AND CONCLUSION

We have shown that by mapping the energy and FWHM of the plasmon peak in the low-loss regime of the EELS spectra, information related to the lattice parameter and the electronic structure of strained III–V semiconductor heterostructures can be obtained with a very high spatial resolution. We have described a simple model of plasmon energy losses in the EELS spectra and have shown that this gives a good fit to the experimentally observed plasmon peaks. Two parameters were extracted from the spectra, namely the plasmon energy E_{max} and FWHM Γ, and used to produce maps of an InAs DWELL structure with nanoscale resolution. We find that the plasmon energy in the quantum well is close to expected values, taking into account the change in lattice parameter of the material. However, the shift in plasmon energy in the dots is much smaller than expected, which may be due to superposition of the matrix plasmon loss on that of the dot. Γ appears to have a maximum value in regions of highest strain gradient in the structure. It is possible to remove the influence of Γ on E_{max} to produce a map of E_p', a parameter related to the average band gap $\bar{E}_g$, the free electron model plasma energy E_p, and the core ion dielectric constant ε_c, and we find that it is possible to describe the shift in plasmon energy as a linear combination of each of these parameters. The dominating factor determining peak shift is the internal strain, which changes E_p via the lattice parameter. The spatial resolution of these maps is of the order of a few nm. Although it is not possible to obtain $\bar{E}_g$, E_p, and ε_c directly from E_p' at present, it seems likely that a more complete analysis will allow these parameters to be mapped individually.

ACKNOWLEDGMENT

The authors would like to acknowledge financial support from EPSRC for many aspects of this program of work.

*Corresponding author: E-mail address: richard.beanland@bookham.com

[1] V. M. Ustinov, A. E. Zhukov, A. Yu Egorov, and N. A. Maleev, *Quantum Dot Lasers* (Oxford University Press, Oxford, 2003).
[2] A. M. Sanchez, G. Nouet, P. Ruterana, F. J. Pacheco, S. I. Molina, and R. Garcia, Appl. Phys. Lett. **79**, 3588 (2001).
[3] M. A. O'Keefe, C. J. Hetherington, Y. C. Wang, E. C. Nelson, J. H. Turner, C. Kisielowski, J. O. Malm, R. Mueller, J. Ringnalda, M. Pan, and A. Thust, Ultramicroscopy **89**, 215 (2001).
[4] S. Kret, P. Ruterana, A. Rosenauer, and D. Gerthse, Phys. Status Solidi B **227**, 247 (2001).
[5] H. Kato, J. Yoshinobu, and M. Kawai, Surf. Sci. **428**, 69 (1999).
[6] E. Carlino, S. Modesti, D. Furlanetto, M. Piccin, S. Rubini, and A. Franciosi, Appl. Phys. Lett. **83**, 662 (2003).
[7] H. Lakner, B. Rafferty, and B. Brockt, J. Microsc. **194**, 79 (1998).
[8] V. J. Keast, A. J. Scott, M. J. Kappers, C. T. Foxon, and C. J. Humphreys, Phys. Rev. B **66**, 125319 (2002).
[9] M. H. Gass, A. J. Papworth, T. J. Bullough, and P. R. Chalker, Ultramicroscopy **101**, 257 (2004).
[10] A. M. Sanchez, M. Gass, A. J. Papworth, P. J. Goodhew, and P. Ruterana, Phys. Rev. B **70**, 035325 (2004).
[11] H. Raether, *Excitation of Plasmons and Interband Transitions by Electrons* (Springer-Verlag, Berlin, 1980).
[12] D. Pines, *Elementary Excitations in Solids* (Benjamin, New York, 1963).
[13] C. Kittel, *Introduction to Solid State Physics* (John Wiley & Sons, Inc., New York, 1996).
[14] R. F. Egerton, *Electron Energy Loss Spectroscopy in the Electron Microscope* (Plenum Press, New York, 1986).
[15] C. Horie, Prog. Theor. Phys. **21**, 113 (1959).
[16] H. Frolich, in *Phenomenological Theory of the Energy Loss of Fast Particles in Solids*, Max Planck Festschrift, edited by W. Framl (Deutscher Verlarg, Berlin, 1958).
[17] M. K. Kundmann, Ph.D. thesis, University of California at Berkeley, 1988.
[18] S. Ossicini, Phys. Status Solidi A **170**, 377 (1998).
[19] J. Stiebling and H. Raether, Phys. Rev. Lett. **40**, 1293 (1978).
[20] R. Manzke, J. Phys. C **13**, 911 (1980).
[21] R. Beanland, Microscopy Today Jan/Feb 2003, p. 29.
[22] T. Grenet and M. C. Cheynet, Eur. Phys. J. B **13**, 701 (2000).
[23] A. C. Ferrari, A. Libassi, B. K. Tanner, V. Stolojan, J. Yuan, L. M. Brown, S. E. Rodil, B. Kleinsorge, and J. Robertson, Phys. Rev. B **62**, 11089 (2000).
[24] T. Hanrath and A. Korgel, Nano Lett. **4**, 1455 (2004).
[25] E. G. Bithell and W. M. Stobbs, Philos. Mag. A **60**, 39 (1989).
[26] E. G. Bithell and W. M. Stobbs, J. Appl. Phys. **69**, 2149 (1991).
[27] *Properties of Gallium Arsenide (EMIS datareview series)*, 3rd ed., edited by M. R. Brozel and G. E. Stillman (Inspec, London, 1990).
[28] A Lorentzian function is clearly a better choice to fit a plasmon peak, but is currently unavailable in EELS analysis software. Energy is unaffected by this difference in fitting function, but both peak intensity and FWHM are slightly underestimated.
[29] H. R. Daniels, R. Brydson, A. Brown, and B. Rand, Ultramicroscopy **96**, 547 (2003).